CHAPTER IV
RESULTS AND DISCUSSION

4.1 Catalyst Characterization

4.1.1 Elemental Analysis

Table 4.1 Elemental analysis of $Ce_{0.75}Zr_{0.25}O_2$

Element	Composition (%wt.)	Theoretical value (%wt.)
Ce	66.08	65.72
Zr	13.43	14.26
O	20.49	20.01

Table 4.2 Elemental analysis of $Ce_{0.75}Zr_{0.15}Mg_{0.20}O_2$

Element	Composition (%wt.)	Theoretical value (%wt.)
Ce	70.64	67.52
Zr	5.45	8.79
Mg	3.28	3.12
O	20.63	20.56

Table 4.3 Elemental analysis of $Ni/Ce_{0.75}Zr_{0.25}O_2$

Element	Composition (%wt.)	Theoretical value (%wt.)
Ni	19.43	15.00
Ce	53.78	55.87
Zr	10.12	12.12
O	16.67	17.01

Table 4.4 Elemental analysis of $Ni/Ce_{0.75}Zr_{0.15}Mg_{0.20}O_2$

Element	Composition (%wt.)	Theoretical value (%wt.)
Ni	18.74	15.00
Ce	55.36	57.40
Zr	4.14	7.47
Mg	3.10	2.65
O	18.66	17.48

Tables 4.1 to 4.4 present the elemental compositions obtained from XRF analysis, expressed as weight percentages, of the investigated supports and catalysts. The nickel contents of both catalysts, $Ni/Ce_{0.75}Zr_{0.25}O_2$ and $Ni/Ce_{0.75}Zr_{0.15}Mg_{0.20}O_2$, were over from the designed value ca. 20 %wt. and similar. The compositions of Ce, Mg and O_2 were consistent with the theoretical value except Zr. In $Ce_{0.75}Zr_{0.15}Mg_{0.20}O_2$ and $Ni/Ce_{0.75}Zr_{0.15}Mg_{0.20}O_2$, it was found that this Zr incorporated into CeO_2 lattices less than the desired values. Zr and Mg could be completely incorporated due to the ionic radius of Zr and Mg is similar ca. 0.72 Å but there are competitive incorporation between Zr and Mg into CeO_2 lattices.

4.1.2 BET Surface Areas and Total Pore Volume

Table 4.5 BET surface areas and total pore volume of the supports and catalysts

Support / Catalyst	Surface Area (m^2/g)	Total Pore Volume (cm^3/g)
$Ce_{0.75}Zr_{0.25}O_2$	159.7	0.54
$Ni/Ce_{0.75}Zr_{0.25}O_2$	149.7	0.24
$Ce_{0.75}Zr_{0.15}Mg_{0.20}O_2$	140.9	0.88
$Ni/Ce_{0.75}Zr_{0.15}Mg_{0.20}O_2$	109.8	0.85

The BET surface areas and total pore volume of prepared supports and catalysts are shown in Table 4.5. The results showed that the BET surface areas and pore volume of supports were decreased after nickel impregnation because the impregnated nickel species dispersed on the surface of support and also blocked some of the support pores (Chen *et al.*, 2008).

4.1.3 H_2-Chemisorption

Table 4.6 Degree of Ni dispersion of the Ni supported catalysts

Catalyst	Ni dispersion (%)
15% $Ni/Ce_{0.75}Zr_{0.25}O_2$	1.86
15% $Ni/Ce_{0.75}Zr_{0.15}Mg_{0.20}O_2$	2.13

Figure 4.6 shows the Ni dispersion of 15% $Ni/Ce_{0.75}Zr_{0.25}O_2$ and 15% $Ni/Ce_{0.75}Zr_{0.15}Mg_{0.20}O_2$. Ni particles more highly dispersed on $Ce_{0.75}Zr_{0.15}Mg_{0.20}O_2$ support so $Ni/Ce_{0.75}Zr_{0.15}Mg_{0.20}O_2$ is expected higher conversion and selectivity.

4.1.4 X-ray Diffraction

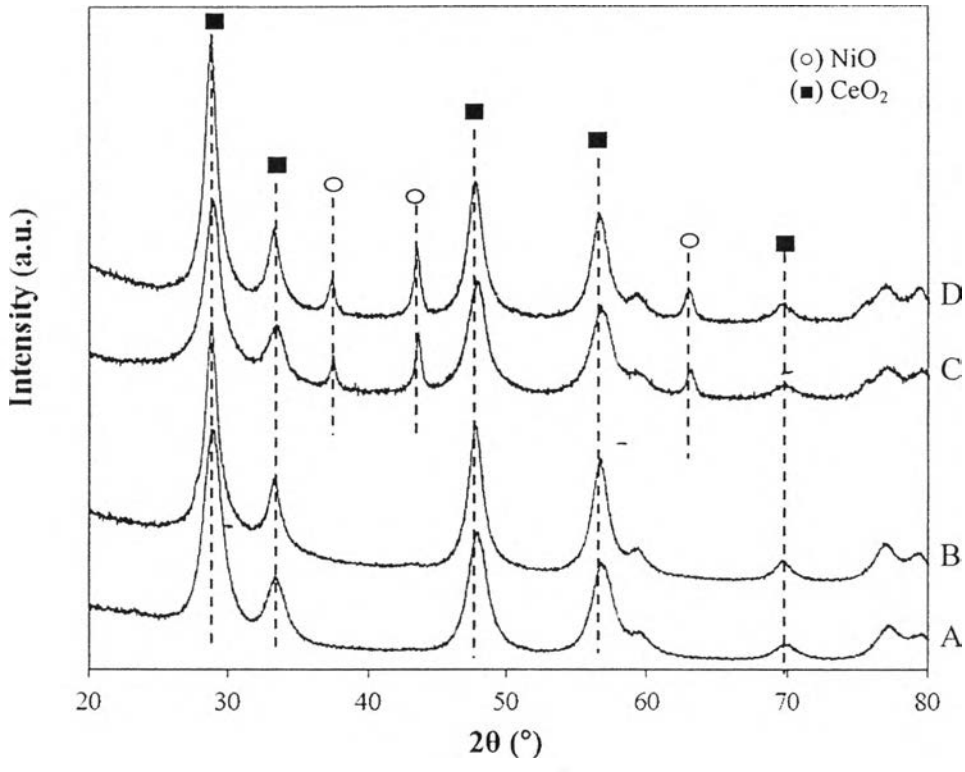

Figure 4.1 XRD patterns of supports and catalysts: (A) $Ce_{0.75}Zr_{0.25}O_2$, (B) $Ce_{0.75}Z_{0.15}Mg_{0.20}O_2$, (C) $Ni/Ce_{0.75}Zr_{0.25}O_2$ and (D) $Ni/Ce_{0.75}Z_{0.15}Mg_{0.20}O_2$.

The crystalline structures of the supports and catalysts were determined by X-ray diffraction as shown in Figure 4.1. For $Ce_{0.75}Zr_{0.25}O_2$ and $Ce_{0.75}Z_{0.15}Mg_{0.20}O_2$, the major peak at ca. 29°, 33°, 48 and 56° (2θ) were observed which represent the indices of (101), (200), (220) and (311) planes, respectively. This indicated a cubic fluorite structure of CeO_2. No extra peaks of non-incorporated ZrO_2 and MgO were appeared, indicating that the atoms of Zr and Mg were incorporated into CeO_2 lattices (Pengpanich *et al.*, 2002) to form a solid solution. For $Ni/Ce_{0.75}Zr_{0.25}O_2$ and $Ni/Ce_{0.75}Z_{0.15}Mg_{0.20}O_2$, the additional peak at ca. 37°, 43° and 62° (2θ) were attributed to NiO species (Pengpanich *et al.*, 2004).

4.1.5 Temperature Programmed Reduction of Hydrogen (H_2-TPR)

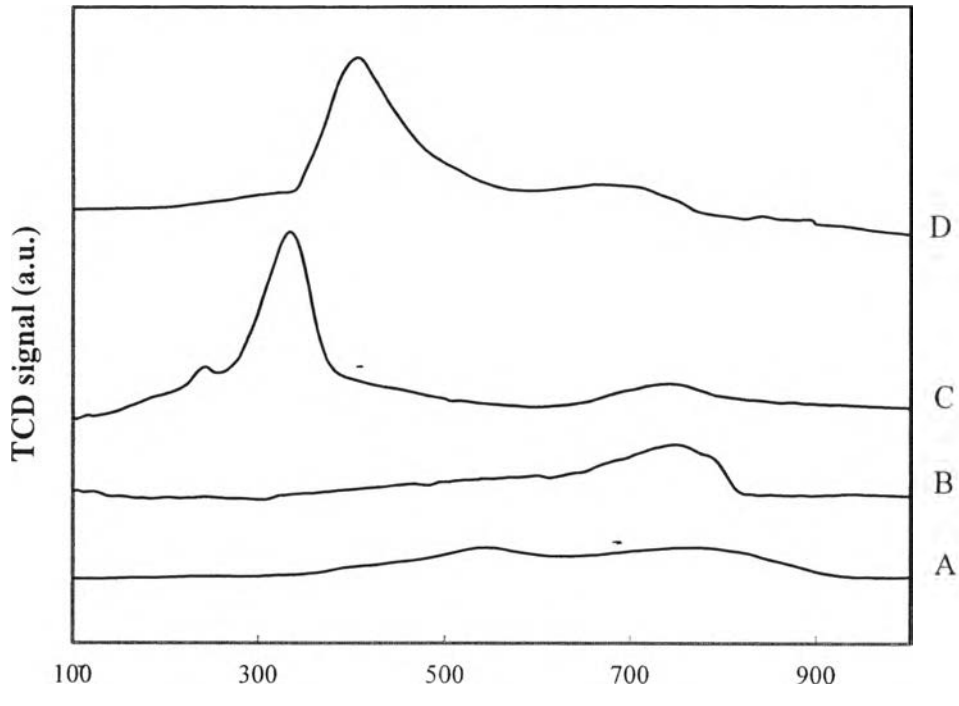

Figure 4.2 H_2-TPR profiles of supports and catalysts: (A) $Ce_{0.75}Zr_{0.25}O_2$, (B) $Ce_{0.75}Z_{0.15}Mg_{0.20}O_2$, (C) $Ni/Ce_{0.75}Zr_{0.25}O_2$ and (D) $Ni/Ce_{0.75}Z_{0.15}Mg_{0.20}O_2$. The reducing gas containing 5% H_2 in Ar with a flow rate 50 ml/min, and a heating rate of 10 °C/min.

H_2-TPR profile of supports and catalysts are shown in Figure 4.2. For $Ce_{0.75}Zr_{0.25}O_2$ support, two broad peaks were observed at ca. 550 °C and 780 °C that were attributed to the reductions of surface oxygen and bulk oxygen, respectively. The additional peak of nickel in $Ni/Ce_{0.75}Zr_{0.25}O_2$ at ca. 240 °C and 330 °C were indicative of the reduction of NiO to Ni^0 of free NiO particles and complex NiO species in intimate contact with the oxide support, respectively, whereas the other peaks of $Ni/Ce_{0.75}Zr_{0.25}O_2$ were assigned to the reduction of support (Thaicharoensutcharittham *et al.*, 2009). For $Ce_{0.75}Zr_{0.15}Mg_{0.20}O_2$ support, only one broad peak was observed at ca. 760 °C that was related to the reduction of bulk oxygen. For 15 %wt. $Ni/Ce_{0.75}Zr_{0.15}Mg_{0.20}O_2$ catalyst, the peak at ca. 400 °C was observed for which it was related to the reduction of complex NiO species.

4.1.6 Temperature Programmed Desorption of Ammonia (NH_3-TPD)

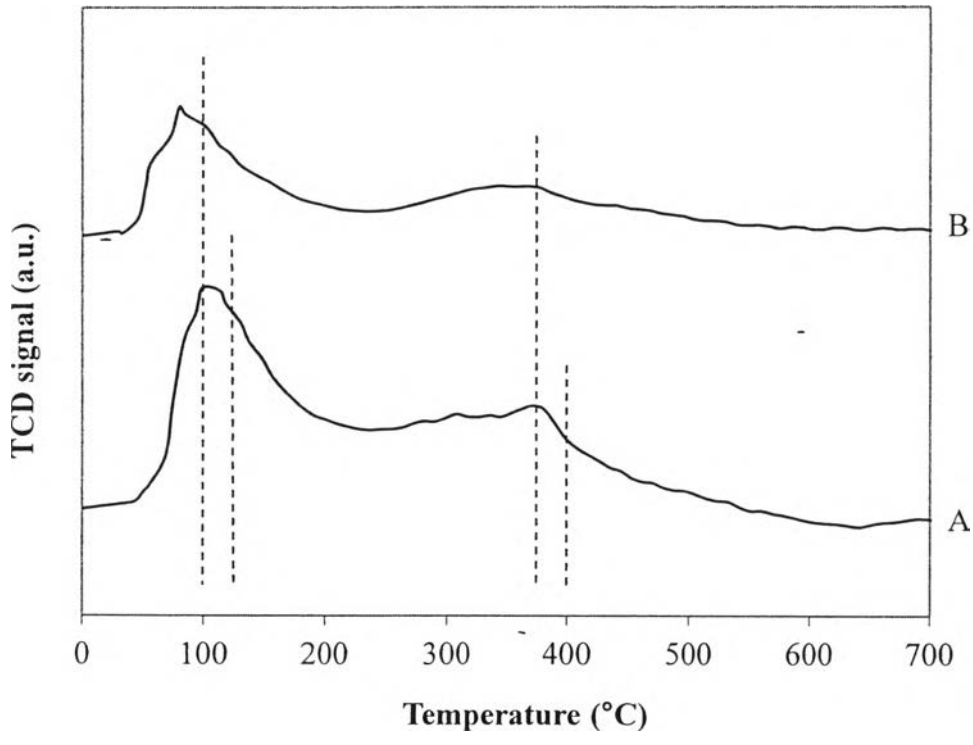

Figure 4.3 NH_3-TPD profiles of (A) $Ce_{0.75}Zr_{0.25}O_2$ and (B) $Ce_{0.75}Z_{0.15}Mg_{0.20}O_2$.

The acidity of supports was determined by NH_3-TPD technique. TPD profiles of $Ce_{0.75}Zr_{0.25}O_2$ and $Ce_{0.75}Z_{0.15}Mg_{0.20}O_2$ supports are shown in Figure 4.3. For $Ce_{0.75}Zr_{0.25}O_2$, two peaks were observed at ca. 100 °C and 370 °C which represent a weak and a medium acid strength, respectively. For $Ce_{0.75}Z_{0.15}Mg_{0.20}O_2$, two peaks were also observed but shifted to lower temperatures at ca. 90 °C and 350 °C. In addition, the peak area of $Ce_{0.75}Z_{0.15}Mg_{0.20}O_2$ was lower than that of $Ce_{0.75}Zr_{0.25}O_2$ indicating that the acidity of $Ce_{0.75}Z_{0.15}Mg_{0.20}O_2$ was lower than that of $Ce_{0.75}Zr_{0.25}O_2$.

4.1.7 Scanning Electron Microscopy (SEM)

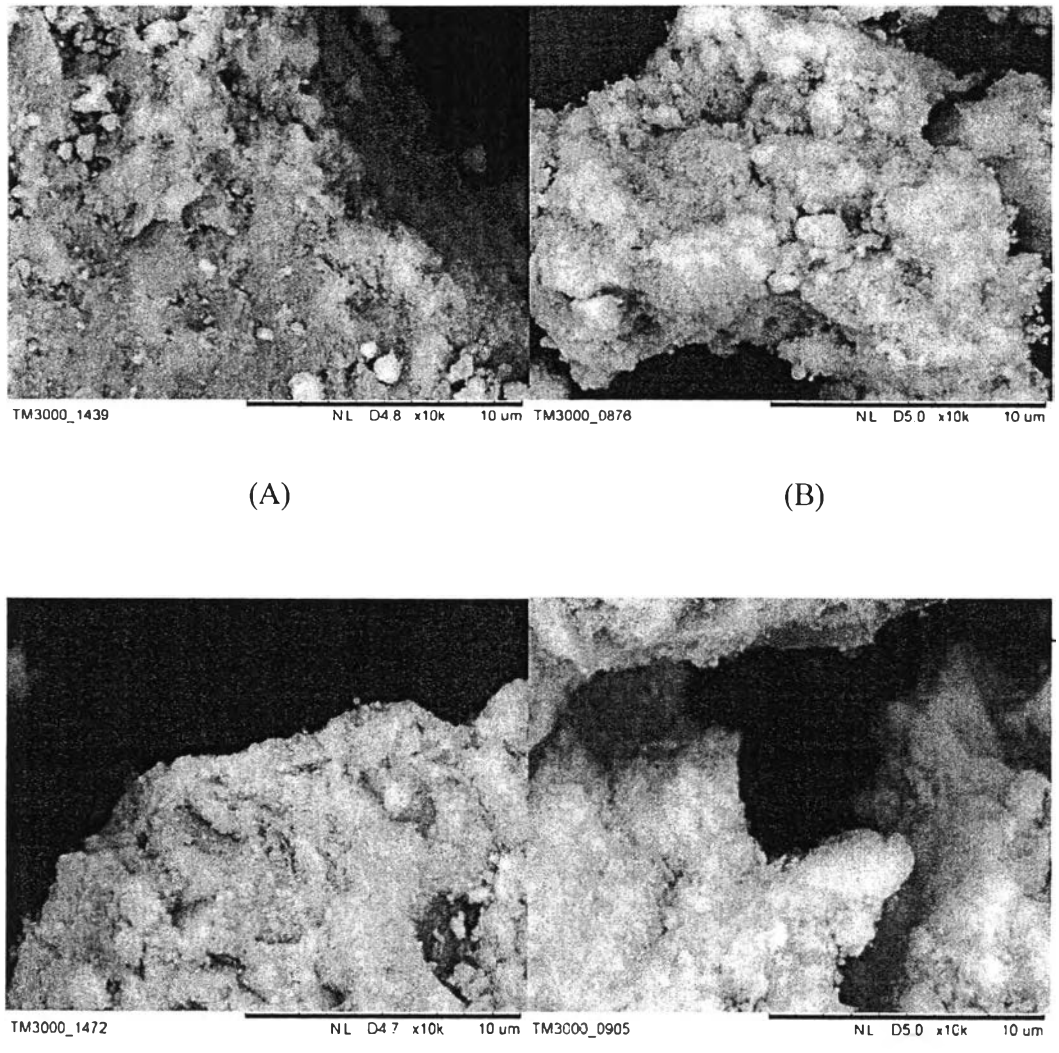

Figure 4.4 SEM images of A) $Ce_{0.75}Zr_{0.25}O_2$, B) $Ni/Ce_{0.75}Zr_{0.25}O_2$, C) $Ce_{0.75}Z_{0.15}Mg_{0.20}O_2$ and D) $Ni/Ce_{0.75}Z_{0.15}Mg_{0.20}O_2$.

Figure 4.4 shows SEM images of supports and catalysts investigated. For the supports, both $Ce_{0.75}Zr_{0.25}O_2$ and $Ce_{0.75}Z_{0.15}Mg_{0.20}O_2$ show an irregular morphology of the ceria-zirconia mixed oxide. After Ni was impregnated, NiO particles attached and distributed onto the surface of supports.

4.2 Catalytic Activities testing

The $Ni/Ce_{0.75}O_{0.25}O_2$ catalyst was further investigated for various effects on its catalytic performance. The results are presented as follows.

4.2.1 Effect of Reaction Temperature

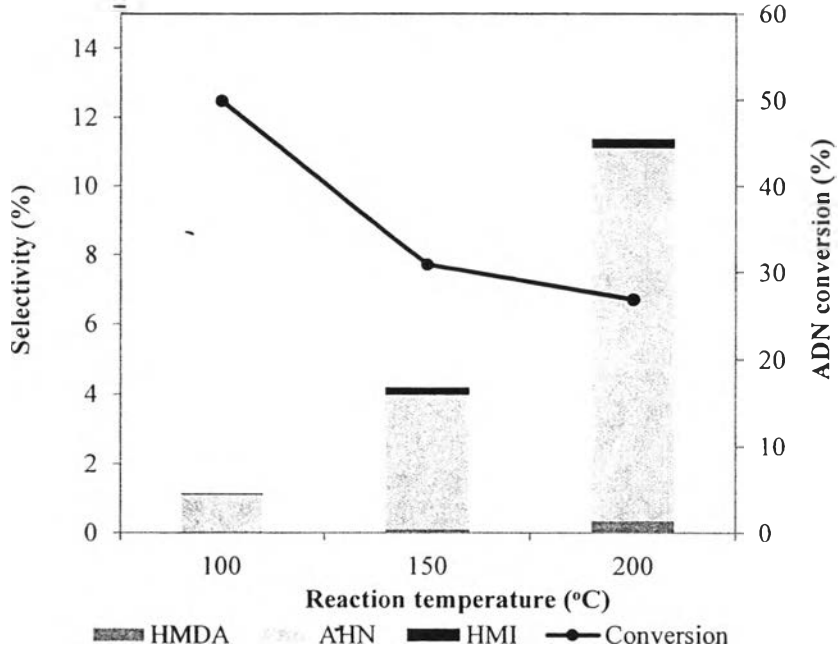

Figure 4.5 ADN conversion and the selectivity of HMDA, AHN and HMI as a function of reaction temperature over the catalysts investigated at H_2/ADN = 120 and 83925 h^{-1}.

Figure 4.5 illustrates the effect of reaction temperatures on the product selectivity and ADN conversion. At reaction temperature 100, 150 and 200 °C, the selectivity of HMDA was ca. 0.02, 0.10 and 0.34%, the selectivity of AHN was ca. 1.09, 3.87 and 10.76% and the selectivity of HMI was ca. 0.03, 0.23 and 0.28% so main product at each reaction temperature was AHN. As an increasing in the selectivity of AHN, HMDA and HMI were also increased due to the deeper hydrogenation of AHN, so it was implied that the production of HMDA, AHN and HMI was favoured at higher reaction temperatures. On the other hand, ADN conversion, decreased with increasing temperatures, was ca. 49.92, 30.85 and

26.83% because adiponitrile hydrogenation is exothermic reaction which is favoured at low temperature.

4.2.2 Effect of Hydrogen to Adiponitrile Mol Ratio (H_2/ADN)

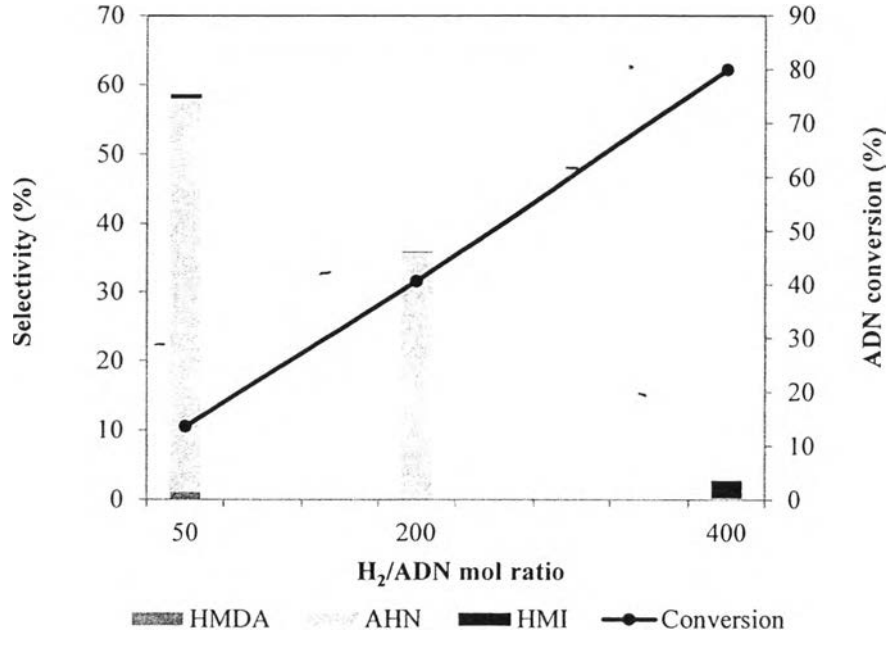

Figure 4.6 ADN conversion and the selectivity of HMDA, AHN and HMI at different H_2/ADN ratio over the catalysts investigated at 200 °C and 93368 h^{-1}.

Figure 4.6 illustrates the effect of hydrogen to adiponitrile mol ratio on the product selectivity and ADN conversion. At H_2/ADN = 50, 200 and 400, the selectivity of HMDA was ca. 1.07, 0.05 and 0.12%, the selectivity of AHN was ca. 56.90, 35.73 and 0.09% and the selectivity of HMI was ca. 0.69, 0.06 and 2.62%. The selectivity of AHN significantly decreased with increasing the H_2/ADN ratio due to the higher H_2/ADN ratio has more molecules of H_2 that can further hydrogenate AHN to HMDA and HMI. It was also observed that the selectivity HMI was higher than HMDA at higher H_2/ADN ratio. These results are in agreement with previous report of Serra and co-workers (2002) by increasing H_2/ADN ratio from 4 to 9 at 200 °C and space velocity 5,968 h^{-1} that the selectivity of HMI and ADN conversion was increased from 23 to 53% and 97 to 100%, respectively while the selectivity of AHN and HMDA were decreased from ca. 23 to 0% and 37 to 17%, respectively.

Although, the formation of HMI theoretically requires the same hydrogen consumption as HMDA, HMI possesses a slower rate of formation and higher thermodynamic stability so the production of HMI was favoured at higher hydrogen amounts (Serra *et al.*, 2002). In this study, ADN conversion was found to increase; ca. 13.57, 40.58 and 79.89%, with increasing H_2/ADN ratio due to the higher H_2/ADN ratio has more molecules of H_2 that can also hydrogenate more ADN.

4.2.3 Effect of Gas Hourly Space Velocity (GHSV)

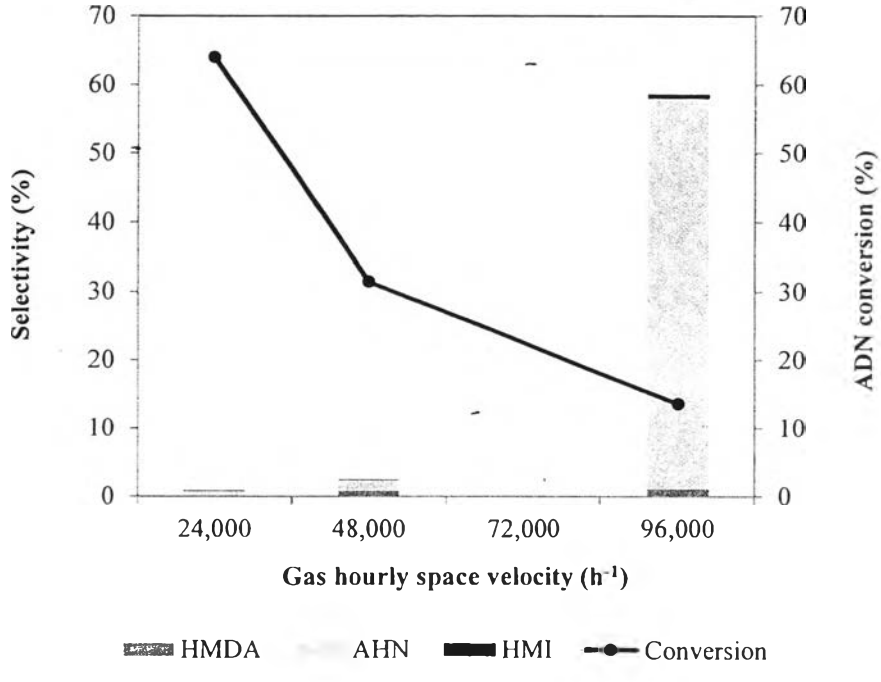

Figure 4.7 ADN conversion and the selectivity of HMDA, AHN and HMI at different GHSV over the catalysts investigated at 200 °C and H_2/ADN = 50.

Figure 4.7 illustrates the effect of GHSV on the product selectivity and ADN conversion. At 24100, 47986 and 93368 h^{-1}, the selectivity of HMDA was ca. 0.17, 0.83 and 1.07%, the selectivity of AHN was ca. 0.63, 1.57 and 56.90% and the selectivity of HMI was ca. 0.01, 0.06 and 0.69%. The selectivity of AHN significantly increased with increasing GHSV due to the fast desorption of AHN generated, thus decreasing the consecutive hydrogenation to HMDA and HMI (Thichit *et al.*, 2002). The selectivity of HMDA was higher than that of HMI

selectivity because HMI has a slower rate of formation as mentioned in the effect of hydrogen to adiponitrile ratio. This result was conformed to the previous work of Serra and co-workers (2002), reported that by increasing GHSV from 23,873 to 71,620 h^{-1} at 150 °C and H_2/ADN = 178. At lower GHSV, the selectivity of HMI (45%) was greater than HMDA (36%) but at higher GHSV, the selectivity of HMDA (67%) was greater than HMI (16%). In this study, it was found that ADN conversion decreased; ca. 64.01, 31.42 and 13.57%, with increasing GHSV from 24100 to 93368 h^{-1}because the higher GHSV means the higher total flow rate of the reaction so ADN has short contact time for the reactions involved to take place.

4.2.4 Effect of Catalyst Acidity

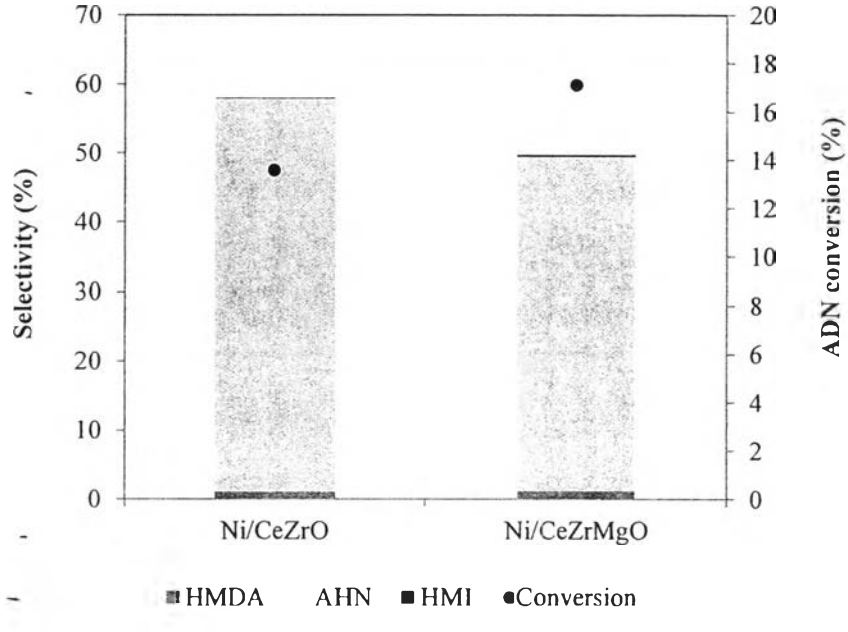

Figure 4.8 ADN conversion and the selectivity of HMDA, AHN and HMI at different catalysts acidity over the catalysts investigated at 200 °C, H_2/ADN = 50 and 93368 h^{-1}.

The previous work of Verhaak and co-workers (1994) showed that the higher basicity of the catalysts can produce more primary amine. The reaction occurred at 125 °C without the addition of ammonia. Potassium was loaded into the catalysts in the different quantity. The higher potassium loading showed the higher

catalyst basicity and induced a higher selectivity of primary amine. It is demonstrated that the more basic catalysts are the ones most selective for the production of primary amine in nitrile hydrogenation (Verhaak *et al.*, 1994) since the basicity can suppress the deammoniation reaction that converts AHN to HMI. In this study, NH_3-TPD profiles (Fig.4.3) confirmed that the addition of magnesium into the support could decrease the acidity of the catalysts. Figure 4.8 shows the effect of acidity on the product selectivity and ADN conversion. AHN was still the main product of both catalysts whereas ADN conversion slightly increased, from ca. 13.57 to 17.11%, with decreasing acidity. The selectivity of HMDA was also increased; from ca. 1.07 to 1.19%, yet that of HMI was decreased; from ca. 0.69 to 0.28%, with decreasing acidity.